Astron. Astrophys. 324, 344–356 (1997)

ASTRONOMY
AND
ASTROPHYSICS

Quantum interferences, hyperfine structure, and Raman scattering on the Sun

J.O. Stenflo

Institute of Astronomy, ETH Zentrum, CH-8092 Zurich, Switzerland

Received 13 November 1996 / Accepted 24 January 1997

Abstract. Observations of the scattering polarization in the solar spectrum have opened a new window for diagnostics of the Sun. In the present paper a theoretical basis for the interpretation of the linearly polarized spectral structures is developed. It covers the general case of Raman scattering for entire atomic multiplets and includes the quantum interferences between the various possible excited states. Although the formulation allows for the presence of magnetic fields of arbitrary strength and direction, the theory is expressed in explicit form only for the case of zero magnetic field. It is applied to identify and interpret observed spectral signatures of quantum interferences between fine structure and hyperfine structure components, isotope effects, and fluorescence within multiplets.

Key words: polarization – scattering – Sun: general – atomic processes – radiative transfer

1. Introduction

A window to a previously unexplored parameter domain has been opened with the availability of an imaging polarimeter system, ZIMPOL (**Z**urich **Im**aging Stokes **Pol**arimeter) (Povel et al. 1991; Keller et al. 1992; Stenflo et al. 1992; Stenflo 1994; Povel 1995), which reaches an accuracy of 10^{-5} in the degree of polarization. At this level of precision the whole solar spectrum is full of polarized spectral structures that are present even in the absence of any magnetic fields, since both the line and continuous spectrum are partly formed by scattering processes. As the illumination of the scattering particles in the solar atmosphere is not entirely isotropic, the incident radiation induces an atomic alignment of the excited states, with the result that the emitted light is partially polarized.

An anisotropy of the incident radiation field is always present even for a spherically symmetric sun due to the limb darkening of the solar disk, but small-scale inhomogeneities, like granulation and magnetic flux tubes, cause local fluctuations. The scattering polarization that is due to the limb-darkening anisotropy is zero at disk center for symmetry reasons and increases monotonically as one approaches the solar limb.

Since the resulting linearly polarized spectrum is very different in appearance and information contents as compared with the ordinary intensity spectrum, it has been found convenient to refer to it as "the second solar spectrum" (Stenflo 1996; Stenflo & Keller 1996a,b).

The prime objective of the present paper is to develop a theoretical framework that can be used to interpret the multitude of spectral structures seen in "the second solar spectrum", since previous theories have been too incomplete, only address certain aspects of the general problem, or do not have a suitable form for practical applications. Although the pioneering work by Landi Degl'Innocenti (1983), extended by Landi Degl'Innocenti et al. (1991a,b), has provided a general theory for Rayleigh scattering in terms of a density matrix formalism, and Bommier (1996) has formulated the partial frequency redistribution problem for Rayleigh scattering in weak magnetic fields to 4th order and higher in quantum perturbation theory, these formulations do not easily lend themselves to practical, exploratory applications. Furthermore the observed polarization is generally not only due to Rayleigh scattering but is in a large number of cases produced by Raman scattering involving many atomic levels with quantum interferences between them. A suitable theoretical framework is needed to address such common cases in a convenient way.

The theory of the present paper is formulated for the general case of Raman scattering (that has Rayleigh scattering as a special case) with atomic coherences in a magnetic field of arbitrary strength and direction, taking into account all the fluorescent contributions within or between the atomic multiplets considered (including hyperfine multiplets). Explicit expressions are however only given for the case of zero magnetic field. Although the theory may be incorporated in a radiative transfer formalism, we bypass in the present paper the radiative transfer problem for exploratory purposes by introducing a parametrized model that is useful for identifying the physical effects and for obtaining model fits to the shapes of the polarized line profiles.

With these tools the underlying physics behind a number of observed spectral structures can then be identified in terms of

Raman and fluorescent scattering within multiplets, quantum interferences between excited states of different total angular momenta, hyperfine structure and isotope effects.

2. Quantum theory of line polarizability

2.1. Introduction

For allowed electric dipole transitions the quantum-mechanical amplitude for scattering from initial substate a to final substate f via the intermediate, excited substates b is given by the Kramers-Heisenberg formula

$$w_{\alpha\beta} \sim \sum_b \frac{\langle f \,|\, \hat{\boldsymbol{r}} \cdot \boldsymbol{e}_\alpha \,|\, b \rangle \langle b \,|\, \hat{\boldsymbol{r}} \cdot \boldsymbol{e}_\beta \,|\, a \rangle}{\omega_{bf} - \omega - i\gamma/2} \,. \tag{1}$$

$\boldsymbol{e}_{\alpha,\beta}$ are the polarization vectors of the radiation field, ω the frequency of the scattered radiation, $\hbar\omega_{bf}$ the energy difference between the upper and final levels, and γ the damping constant (which is the sum of the radiative and collisional contributions). The summation is done over all the intermediate states b. Since energy conservation requires that $\omega_{bf} - \omega = \omega_{ba} - \omega'$, we could also express Eq. (1) in terms of the frequencies ω' of the incident radiation.

The radiation coherency matrix $\boldsymbol{W}$ that describes the transformation from the polarization state of the incident to that of the scattered radiation is given by

$$\boldsymbol{W} = \sum_{\mu_a} \sum_{\mu_f} \boldsymbol{w} \otimes \boldsymbol{w}^* \tag{2}$$

(Stenflo 1994), where the symbols $\otimes$ and $*$ stand for tensor product and complex conjugation, respectively. For simplicity we have here assumed (as we will do in the rest of the paper) that there is no atomic polarization in the initial state a when summing over all the initial and final magnetic substates that are represented by their magnetic quantum numbers $\mu_{a,f}$. This allows us to express the polarizing characteristics of the scattering process in terms of a phase matrix (see below) that is independent of the scattering medium (the model atmosphere used) and only depends on atomic physics. The neglect of the polarization of state a is physically well justified because the life time of the initial state with respect to radiative absorption processes is longer than the radiative life time of the excited state by about two orders of magnitude (cf. Sect. 4). The initial state therefore has plenty of time to be depolarized by collisions and weak magnetic fields.

Note that the initial, intermediate, and final states may have arbitrary Zeeman splittings, and that ω_{bf} in Eq. (1) contains the Zeeman displacements of the magnetic sublevels b and f. The formulation therefore allows for magnetic fields of arbitrary strengths.

To obtain the scattering Mueller matrix $\boldsymbol{M}$ that describes how a Stokes 4-vector is transformed by the scattering process, we form

$$\boldsymbol{M} \sim \boldsymbol{T}\,\boldsymbol{W}\,\boldsymbol{T}^{-1} \,, \tag{3}$$

where $\boldsymbol{T}$ is a purely mathematical transformation matrix without physical contents, given explicitly in Stenflo (1994). The constant of proportionality is determined by the normalization condition for $\boldsymbol{M}$.

We may expand $\boldsymbol{M}$ in terms of its multipolar components (Stenflo 1996):

$$\boldsymbol{M} = \sum_{K=0}^{2} \boldsymbol{M}_K \,, \tag{4}$$

where index K represents the $2K$-multipole. Let us by $\boldsymbol{E}_{ij}$ define a 4×4 matrix that has its ij component equal to unity, while all the other components are zero. Then, in the limit of weak magnetic fields, defined by the requirement that the Zeeman splitting should be much smaller than the Doppler broadening, $\boldsymbol{M}_0 \sim \boldsymbol{E}_{11}$, while $\boldsymbol{M}_1 \sim \boldsymbol{E}_{44}$. This means that $\boldsymbol{M}_0$ represents isotropic, unpolarized scattering, while $\boldsymbol{M}_1$ only scatters the circular polarization, which in this limit is decoupled from the linear polarization. Thus the scattered radiation contains circular polarization only if the incident radiation also contains circular polarization. In contrast, unpolarized incident light is the main source of linear polarization in the scattered radiation. Therefore the study of scattering physics focuses on the linear polarization, which is generated by the $\boldsymbol{M}_2$ matrix.

In the weak-field limit the effect of the Zeeman splitting on the shapes of the absorption line profiles can be disregarded. This means that all the matrix components of $\boldsymbol{M}$ can be assumed to have the same frequency profile, which therefore can be factorized out from $\boldsymbol{M}$ as a common scalar. The remaining, frequency-independent matrix that describes the polarization properties of the scattering process is in its normalized form the so-called *phase matrix* $\boldsymbol{P}$. It can be expanded as

$$\boldsymbol{P} = \sum_{K=0}^{2} W_K \,\boldsymbol{P}_K \,, \tag{5}$$

where, in the case of zero magnetic fields, $\sum_{K=0}^{2} \boldsymbol{P}_K$ is the classical, Rayleigh scattering phase matrix. By definition and normalization $W_0 = 1$ and $\boldsymbol{P}_0 = \boldsymbol{E}_{11}$. While $W_{1,2} = 1$ for classical scattering the values of these coefficients generally depend on the total angular momentum quantum numbers of the initial, intermediate, and final states a, b, and f. All the quantum-mechanical effects on the scattering process are thus hidden in the W_K coefficients.

When the magnetic field is weak but not zero it influences the scattering process via the *Hanle effect*. Explicit expressions for the $\boldsymbol{P}_K$ matrices in the presence of the weak-field Hanle effect (when the Zeeman splitting is much smaller than the Doppler width) were first given in Stenflo (1978) (cf. also Stenflo 1994).

If we disregard the here unimportant circular polarization, the phase matrix that results from Eq. (1) can in the case of zero magnetic field be written as

$$\boldsymbol{P} = W_2 \,\boldsymbol{P}_R + (1 - W_2)\,\boldsymbol{E}_{11} \,, \tag{6}$$

where $\boldsymbol{P}_R$ is the Rayleigh phase matrix that is valid for the case of classical dipole scattering. W_2 thus represents the fraction of

scattering processes that occurs as classical dipole scattering, while the remaining fraction, $1 - W_2$, represents unpolarized, isotropic scattering.

2.2. Raman scattering with quantum interferences

In the present paper the terms *fluorescent* scattering and *Raman* scattering will both be used to describe cases when the initial and final states are different. The term fluorescent scattering is used when the excitation occurs near an actual resonance, while Raman scattering can occur at frequencies that are arbitrarily far from the resonant frequencies. Raman scattering is therefore the more general concept and approaches continuously the case of fluorescent scattering when we move closer in frequency towards a resonance. Similarly *Rayleigh* and *resonant* scattering both refer to the case when the initial and final states are the same, but while resonant scattering occurs near a resonance, Rayleigh scattering does not have this restriction. In this sense all the three terms fluorescent, Rayleigh, and resonant scattering can be considered to be special cases of Raman scattering (if we consider the case when the initial and final states are identical as a special case of Raman scattering).

The scattering theory developed in the present paper is valid for general Raman scattering. The other terms will be used when addressing special cases.

Let us now in what follows for convenience of notation let a, b, and f refer not as before just to the individual magnetic substates, but instead to the states that are characterized by their total angular momentum quantum numbers (and thus contain magnetic substates, which may in principle be Zeeman shifted). For a given af combination of initial and final states in the limit of weak magnetic fields we may express the Raman scattering Mueller matrix $\boldsymbol{M}_{af}$ as

$$\boldsymbol{M}_{af} \sim \sum_{K=0}^{2} C_{af}^{(K)}\, \boldsymbol{P}_K\,. \tag{7}$$

The coefficients $C_{af}^{(K)}$, which are frequency dependent (see below), contain not only the squared terms but also the interference terms between the various intermediate states of different total angular momenta. Eq. (7) allows us to define a phase matrix of the form (5) if we let

$$W_K = C_{af}^{(K)} \,/\, C_{af}^{(0)}\,. \tag{8}$$

If more than one intermediate state contributes to the transition from state a to state f, W_K will in general be frequency dependent.

The coefficients $C_{af}^{(K)}$ can more explicitly be given as

$$C_{af}^{(K)} = \mathrm{Re} \sum_{m,n} g(a,f)_{mn}\;\; c(a,f)_{mn}^{(K)}\;\; \Phi_{mf}\, \Phi_{nf}^{*} \tag{9}$$

(cf. Stenflo 1994), where m and n label the intermediate states. The coefficients $c(a,f)_{mn}^{(K)}$ depend exclusively on the total angular momentum quantum numbers of levels a, m, n, f. The complex profile function Φ is given by

$$\Phi_{nf} \sim \frac{1}{\omega_{nf} - \omega - i\gamma/2}\,, \tag{10}$$

while

$$g(a,f)_{mn} = (-1)^r \sqrt{f_{am}\, f_{fm}\, f_{an}\, f_{fn}}\,. \tag{11}$$

Here the exponent r is 0 or 1 (thus determining the sign of the expression) depending not only on the total angular momentum quantum numbers J of all the four levels a, m, n, f involved, but also on their respective orbital angular momentum quantum numbers L (in the case of hyperfine structure splitting J, L, S are replaced by F, J, I). The f_{am} etc. in Eq. (11) are the respective absorption oscillator strengths. Their relative values within a multiplet have been given as algebraic expressions of the L, S, and J quantum numbers in Condon & Shortley (1970). Algebraic expressions for the coefficients $c(a,f)_{mn}^{(K)}$ and the exponent r have been derived and given in Stenflo (1994) and are reproduced in the Appendix in a form that is adapted to the somewhat different notations that we have used here. Chapter 9 of Stenflo (1994) explains how these expressions can be derived from sums of products of 3-j symbols for any $K = 0, 1, 2$ (although the less important $K = 1$ case has not been dealt with explicitly yet).

The off-diagonal terms in Eq. (9) represent quantum mechanical interferences between states with different values of $J = J_m$ and J_n. For $K = 0$ such terms cancel out, so that we get

$$C_{af}^{(0)} = \sum_{n} f_{an}\, f_{fn}\; c(a,f)_{nn}^{(0)}\;\; |\Phi_{nf}|^2\,. \tag{12}$$

Quantum interferences between excited states of different total angular momenta can only be neglected when the line opacity becomes much smaller than the continuum opacity at distances from the resonant frequencies that are comparable to the fine structure splitting. In many cases this condition is not at all satisfied, e.g. in the case of the Ca II H and K lines at 3965 and 3933 Å, the Na I D_1 and D_2 lines at 5895.94 and 5889.97 Å, or for the hyperfine structure splitting in lines like Ba II 4554 Å, as we will see below. If only a single excited state b with $J = J_b$ needs to be considered, e.g. when we are at a resonance frequency,

$$W_{K,\,\mathrm{single}} = c(a,f)_{bb}^{(K)} \,/\, c(a,f)_{bb}^{(0)}\,. \tag{13}$$

The diagonal coefficients are given by

$$c(a,f)_{bb}^{(K)} = \left\{ \begin{array}{ccc} 1 & 1 & K \\ J_b & J_b & J_a \end{array} \right\} \left\{ \begin{array}{ccc} 1 & 1 & K \\ J_b & J_b & J_f \end{array} \right\}\,, \tag{14}$$

where the brackets denote 6-j symbols (cf. Landi Degl'Innocenti 1984; Stenflo 1994). Simple, explicit algebraic expressions have been given by Chandrasekhar (1950) for the resonant case $J_f = J_a$ and by Stenflo (1994) for the non-resonant (fluorescent or Raman) case $J_f \neq J_a$.

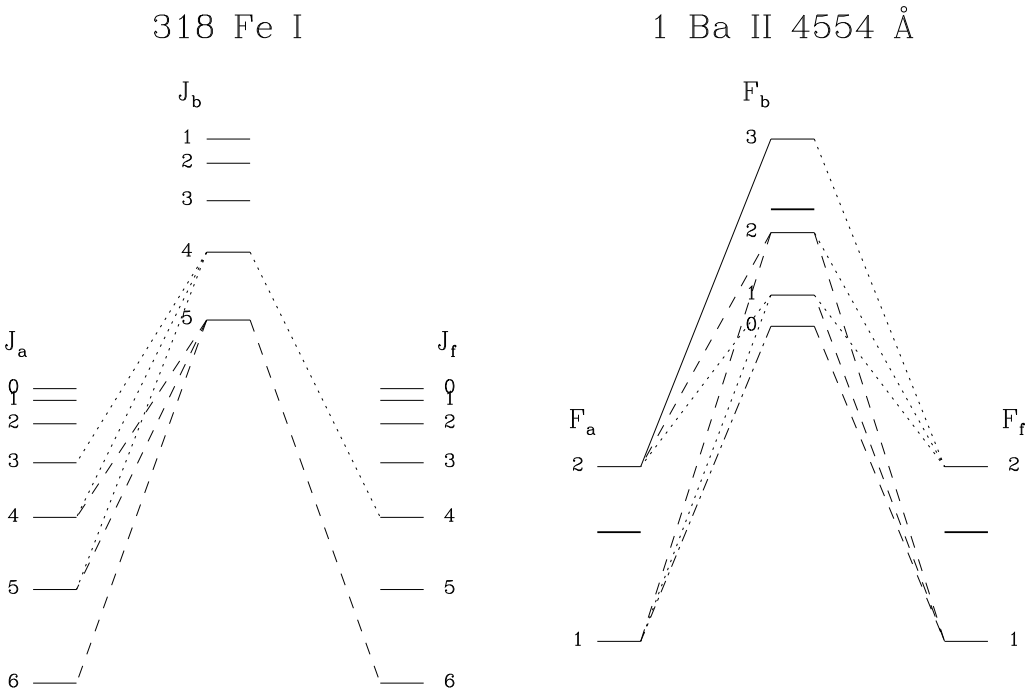

Fig. 1. Energy level diagrams to illustrate scattering transitions in multiplet 318 of Fe I and in the hyperfine multiplet of the Ba II 4554 Å transition. While the relative level shifts within a group of initial (index a), intermediate (index b), or final (index f) states are in the right proportions, we have applied different magnifications to clearly see the levels in the plot. As the hyperfine splitting is so tiny, the energy differences within the F_b group have been magnified by the factor 42,370 with respect to the energy scale for the J_b group, while the corresponding magnifications for the F_a and J_a groups are 3,390 and 2.5, respectively. Thus the upper level hyperfine splitting in Ba II has been magnified by the factor 12.5 with respect to the lower level splitting. The three thick, unlabeled horizontal lines in the Ba II diagram mark the level positions in the absence of hyperfine splitting. Examples of some allowed fluorescent scattering transitions are drawn and are commented on in the text. Note that for 318 Fe I the energy levels *decrease* with increasing value of J.

2.3. Polarizability for an entire multiplet

To obtain the polarizability W_2 for an entire multiplet one has to extend the sums in Eq. (2) over all the possible initial and final states of the multiplet, i.e., one has to add together all the possible fluorescent or Raman scattering contributions within the multiplet. Thereby one needs to account for the multiplicity $(2J + 1)$ of these states, which represents the number of magnetic substates for a given J state (in the case of fine-structure splitting). The emission probability from a given excited state scales with $2J_f + 1$, while the absorption probability scales with the relative population $2J_a + 1$ of the initial states. Effectively it means that the oscillator strengths f in Eq. (11) get replaced by their gf values (g being the statistical weight). Thus the scattering matrix for the whole multiplet becomes

$$\boldsymbol{M} = \sum_{a,f} (2J_a + 1)(2J_f + 1)\, \boldsymbol{M}_{af}\,, \tag{15}$$

where $\boldsymbol{M}_{af}$ is given by Eqs. (1)-(3) in the case of arbitrary Zeeman splitting, and by Eq. (7) in the case of weak magnetic fields. The above as well as the following expressions are valid for multiplets produced by fine-structure splitting. For a hyperfine structure multiplet the expressions remain the same if we replace J with the total angular momentum quantum number F.

If we introduce a phase matrix as in Eq. (5) with the same normalization as before but now representing the whole multiplet, and define

$$C^{(K)} = \sum_{a,f} (2J_a + 1)(2J_f + 1)\, C^{(K)}_{af}\,, \tag{16}$$

then the polarizability coefficients W_K become

$$W_K = C^{(K)} / C^{(0)}\,. \tag{17}$$

In the general case when the incident radiation is not spectrally flat one has to apply the intensity as an additional weight to the nominator and denominator of Eq. (17). Also $C^{(K)}$ in Eq. (16) needs to be convolved with a Gaussian to account for the thermal and turbulent Doppler broadening before it is inserted in the nominator and denominator of Eq. (17) to form W_K.

Fig. 1 shows the energy level diagrams for two multiplets that we will be dealing with, fine structure multiplet No. 318 of neutral iron, and the hyperfine multiplet of the Ba II 4554 Å line. The solid, dashed and dotted lines show some of the different possible combinations of fluorescent scattering transitions in these multiplets.

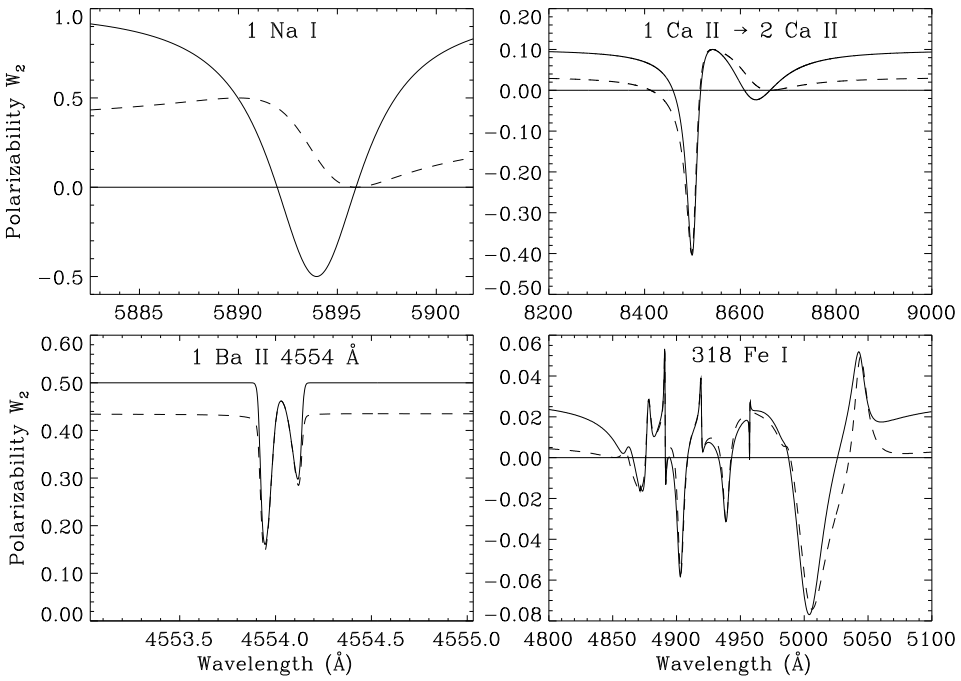

Fig. 2. The polarizability W_2 when accounting for all the allowed Raman scattering transitions within the multiplets 1 Na I and 318 Fe I, between the two multiplets 1 Ca II and 2 Ca II, and within the hyperfine structure multiplet of the 1 Ba II 4554 Å line. The solid curves represent the full solutions, while the dashed curves show what happens if we ignore the quantum interferences between states of different total angular momenta. Only when the interference terms are taken into account we get the asymptotic behavior that is demanded by the principle of spectroscopic stability.

If we sum up all the allowed fluorescent combinations with Eq. (16), then Eq. (17) gives us a polarizability W_2 that can have a very complex wavelength dependence, as shown by Fig. 2, in which the two multiplets of Fig. 1 are represented by the two lower panels. The upper panels represent respectively scattering in the Na I D_1–D_2 multiplet and Raman scattering from the ultraviolet Ca II H and K multiplet No. 1 (at 3965 and 3933 Å) into the infrared multiplet No. 2 of Ca II. While the solid curves give the full solutions, the dashed curves show what happens when the interference terms are left out and only the diagonal contributions to $C_{af}^{(K)}$ in Eq. (9) are used. The Ba II diagram has been constructed as a sum of the different isotopic contributions, and Doppler and instrumental broadening have been applied, in preparation for the later comparison with the observations in Fig. 7 (cf. Sect. 3.4).

2.4. Interference and spectroscopic stability

The principle of spectroscopic stability provides us with a powerful tool to check the correctness of our algorithms to compute the polarizability. In the present context we use this principle to determine what must happen in the limit of vanishing fine (or hyperfine) structure splitting. The fine structure is physically due to the electron spin, so the polarizability W_2 in the limit of vanishing splitting is simply obtained by letting the spin quantum number S be zero, which means that we use $J = L$ in Eq. (14) for $c(a, f)_{bb}^{(K)}$. This limiting value of W_2 must be reached asymptotically when moving away in the spectrum to distances from the resonant wavelengths that are much larger than the wavelength separations between the fine structure components, since at such distances the splitting loses its importance.

Let us use this principle to check the results of Fig. 2. The 1 Na I multiplet represents a transition for which $L = 0 \rightarrow 1 \rightarrow 0$. With $J = L$ in Eq. (14) we find that $W_2 = 1$. The solid curve indeed approaches unity asymptotically when moving either to smaller or larger wavelengths. A $0 \rightarrow 1 \rightarrow 0$ transition is the quantum-mechanical analog to classical dipole-type scattering, for which W_2 of course always has its classical value, unity.

The 1 Ca II $\rightarrow$ 2 Ca II transition corresponds to $L = 0 \rightarrow 1 \rightarrow 2$. This gives the asymptotic value $W_2 = 0.10$, in agreement with the solid curve. Similarly, as the 318 Fe I multiplet is an $^7\mathrm{F}^\circ \rightarrow ^7\mathrm{D} \rightarrow ^7\mathrm{F}^\circ$ transition, we have $L = 3 \rightarrow 2 \rightarrow 3$, which gives $W_2 = 3/105 = 0.0286$, in agreement with the figure.

In the hyperfine case of the Ba II 4554 Å line we have to let the nuclear spin I, which for the odd Ba isotopes is 1.5, go to zero, so that F becomes equal to J. As $J = \frac{1}{2} \rightarrow \frac{3}{2} \rightarrow \frac{1}{2}$, for which $W_2 = 0.5$, this is the asymptotic value, in agreement with the figure.

The dashed curves in Fig. 2 show the solutions for W_2 that are obtained if all the quantum interference (off-diagonal) terms in Eq. (9) are omitted. The asymptotic behavior is then entirely different and violates the principle of spectroscopic stability.

The oscillator strengths f and the sign factor $(-1)^r$ in Eq. (11) are complicated functions of all the quantum numbers J, L, and S (or F, J, and I in the hyperfine case). If any one of these algebraic expressions or those for the coefficients $c(a, f)_{mn}^{(K)}$ would contain an error or a wrong sign, this would immediately show up as a violation of the principle of spectroscopic stability for some combinations of the quantum numbers. We have let our computer program scan through all possible combinations of quantum numbers to verify that the principle of spectroscopic stability is always obeyed.

The principle of spectroscopic stability can be shown to be obeyed also for scattering from each separate initial J_a state, before summing in Eq. (16) over J_a (but after summing over

the final J_f states). This is an even more restrictive condition that the algebraic expressions have to satisfy.

3. Modelling the observed polarization

3.1. Effective polarizability

The observed linear polarization depends on a number of factors: (i) The atomic polarizability coefficient W_2. (ii) The fraction of the emission processes that represent actual scattering transitions. (iii) The "geometric depolarization" factor, determined by the degree of anisotropy of the incident radiation field. (iv) The collisional depolarization factor, i.e., the fraction of the scattering processes that are undisturbed by depolarizing collisions. (v) The Hanle depolarization factor, which expresses how the polarization amplitudes are reduced in the presence of magnetic fields.

There are however many contributors to the solar photons that we observe, including the continuous spectrum and atomic transitions of various other elements. The continuum is weakly polarized due to Thomson scattering at free electrons and Rayleigh scattering at neutral hydrogen. Radiative scattering does not play a significant role in all atomic transitions. Non-scattering lines may depolarize the continuum by removing polarized photons and diluting the continuum radiation with unpolarized photons.

To obtain a representation of the polarization that we can expect to observe from a given atomic multiplet we need to add the contributions from the continuum and from the considered line multiplet, weighted according to the relative number of photons they deliver, i.e., according to the photon emission probability functions. For a given multiplet the photon emission probability is proportional to $C^{(0)}$ of Eq. (16) after it has been convolved by a Gaussian due to thermal and turbulent Doppler broadening. Let us denote this convolved and area-normalized $C^{(0)}$ function by $\phi_I(\nu)$. We note that ϕ_I is in general, as shown by Eqs. (16), (12), and (10), a composite of several different Voigt profiles with different weights and central frequencies.

The corresponding function for the continuum is spectrally flat and can be represented by a constant a, the value of which depends on the magnitude of the continuum opacity relative to the line opacity of the considered multiplet. If we ignore the contributions from other spectral lines we can define an "effective" value of W_2 that represents the weighted sum of the line and continuum contributions (Stenflo 1980):

$$W_{2,\,\mathrm{eff}}(\nu) = W_2(\nu)\,\frac{\phi_I(\nu)}{\phi_I(\nu)+a} + b\,\frac{a}{\phi_I(\nu)+a}\,. \qquad (18)$$

The additional free parameter b represents the relative continuum polarization, which scales with the fraction of continuum emission processes that represent scattering transitions.

To obtain a fit of the observed polarization curves we have to multiply $W_{2,\,\mathrm{eff}}$ with a scale factor that contains the various factors (ii)-(v) mentioned above. In general the factors (iii)-(v) are wavelength dependent, in particular the geometric depolarization factor, and radiative transfer is needed to determine how these factors vary. However, it turns out to be a good approximation for a qualitative discussion of the physics involved to bypass radiative transfer and simply assume that the combined geometric, collisional, and Hanle depolarization factors as well as the incident radiation are spectrally flat over the selected wavelength range. In this case we may obtain the synthetic polarization profile as a function of wavelength directly from $W_{2,\,\mathrm{eff}}$ after applying a global, wavelength-independent scale factor.

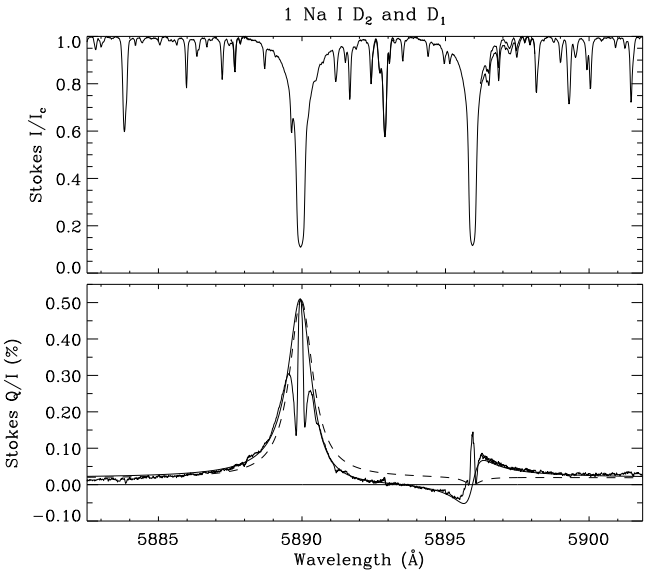

Fig. 3. Modelling the observed quantum interference pattern in multiplet No. 1 of sodium. While the upper panel gives the intensity spectrum I, normalized to the intensity I_c of the local continuum, the lower panel gives the degree of linear polarization, Q/I. Positive values mean that the electric vector of the scattered radiation is preferentially oriented parallel to the nearest solar limb, while negative values represent the orthogonal direction. The thin solid curve was recorded in April 1995 with the ZIMPOL I polarimetric system at the National Solar Observatory (Kitt Peak) with the spectrograph slit 5 arcsec inside the limb at the north pole of the Sun. The thick solid and dashed curves have been obtained by theoretical modelling, the solid with and the dashed without taking the quantum interferences into account.

With a full radiative transfer treatment there would be no free parameters, since their values would be uniquely determined by the model atmosphere used. Our parametrization is introduced to allow us to make useful interpretations while bypassing radiative transfer. It is possible to extend the parametrized model and require that it should simultaneously also fit the wings of the Stokes I profile. This additional constraint would fix the value of the parameter a and remove it from its status as a free parameter (Faurobert-Scholl, private communication). As however such an extension of the model is non-trivial and would involve the use of the Eddington-Barbier relation, it is outside the scope of the present paper.

To summarize, our idealized model for the observed polarization that bypasses radiative transfer thus has three free

parameters: the relative continuum opacity a, the continuum polarization parameter b, and the global scale factor.

3.2. Modelling quantum interferences in sodium

Fig. 3 shows an application of this model to explain the observed polarization profile across the Na I D_1 and D_2 lines that make up multiplet No. 1 of Na I. While the thin solid curve is the observed one (5 arcsec inside the limb at the north pole of the Sun), the thick solid and dashed curves have been obtained from the corresponding solid and dashed W_2 curves in the upper left panel of Fig. 2, using Eq. (18) with $a = 24.5$, $b = 0.018$, and a scale factor of 1.01% . Here a is given in units of the value that ϕ_I has at the wavelength halfways between the two resonant frequencies. While the dashed curve without the quantum interferences is unable to reproduce the sign reversals of the polarization curve around the D_1 line for any combination of the free model parameters, the solid curve provides a surprisingly good representation of the gross features of the observed curve, apart from the narrow spectral features in the two line cores.

A sign reversal means that the electric vector of the scattered radiation, which for positive polarization is oriented parallel to the nearest solar limb, changes its orientation by 90°. This sign reversal is a typical quantum interference effect, in the present case due to coherent superposition of the states with total angular momentum quantum numbers $J = \frac{1}{2}$ and $\frac{3}{2}$. The same phenomenon has been observed and modeled for the Ca II H and K lines at 3965 and 3933 Å (Stenflo 1980), which have the same quantum numbers as the D_1 and D_2 lines.

For Rayleigh scattering the polarizability can never be negative unless there is quantum interference. If the resonant frequencies of the D_1 and D_2 lines are ν_1 and ν_2, the polarizability of the Na I transition as determined by Eq. (8) is

$$W_2 = \frac{(\nu_2 - \nu)^{-2} + 2(\nu_1 - \nu)^{-1}(\nu_2 - \nu)^{-1}}{(\nu_1 - \nu)^{-2} + 2(\nu_2 - \nu)^{-2}} \, . \qquad (19)$$

To simplify the expression we have omitted the damping constant γ, which is allowed since it is unimportant when the fine-structure splitting is so much larger than the damping width. Expression (19) shows explicitly that the source of the negative sign is exclusively in the interference term in the nominator.

The modelling in Fig. 3 ignores the hyperfine structure in sodium, so it is natural to expect that the narrow polarization features in the line cores that are not reproduced by our model could be due to hyperfine structure effects. However, we have performed corresponding model calculations for the hyperfine structure multiplets of the D_2 and D_1 transitions without being able to come close to fitting the core polarization peaks, in spite of the great success of the same theory when applied to the hyperfine structure multiplet of the Ba II 4554 Å line, as we will see below. Thus it appears unlikely that hyperfine structure can have much to do with the narrow polarization peaks of sodium.

The general shape of the D_2 profile, with a narrow core peak surrounded by minima followed by wing maxima, is the same as previously found for the Ca I 4227 Å and Ca II K 3933 Å lines (Stenflo et al. 1980, 1983a,b), which have no hyperfine structure (calcium has zero nuclear spin). It has been possible to explain these types of polarization profiles in terms of partial redistribution effects in polarized radiative transfer (Rees & Saliba 1982; Saliba 1985; Frisch 1996). Therefore it appears likely that the D_2 line can be explained in this way as well, but solutions of the radiative-transfer problem would be needed to prove this point.

For the D_1 line, on the other hand, frequency redistribution within this line is unlikely to provide an explanation of the narrow polarization peak, since the polarizability W_2 near the D_1 resonance is close to zero, and the hyperfine splitting does not seem capable of changing the polarizability sufficiently. Then the frequency redistribution process does not seem to have the building blocks out of which a polarization peak could be constructed.

Interestingly, the two 1 Ba II lines at 4554 and 4934 Å have the same quantum numbers and hyperfine structure patterns (although the magnitudes of the splittings are different) as the 1 Na I D_2 and D_1 lines. The "D_1-type" line Ba II 4934 Å is also observed to have a sharp, pronounced polarization peak, which supports the reality of the Na I D_1 peak and indicates that they have a common, yet unidentified, physical origin. For the Ba II line pair the fine structure splitting is so large (380 Å) that quantum interference from the D_2 transition at 4554 Å cannot play a significant role. Thus new physics not covered by the present theoretical framework may be needed to explain the narrow D_1 polarization peaks of Na I and Ba II.

3.3. Signatures of fluorescent scattering

Let us now turn to multiplet No. 318 of Fe I, which according to Fig. 1 has a complex fine structure splitting pattern with a rich variety of possible fluorescent scattering combinations within the multiplet, which as seen in the lower right panel of Fig. 2 results in a complex structure for the polarizability W_2. The various combinations of energy levels lead to several doublet lines. Two such pairs are shown in the left and right panels of Fig. 4. Both have a complex polarization structure. Here we will focus the discussion on the 4957 Å line pair, since its polarization feature has remained an unexplained riddle since it was first observed with a Fourier transform spectrometer in 1978 (Stenflo et al. 1983b). Only now it can be demonstrated that it is a signature of fluorescence within the multiplet, as will be shown below.

Fig. 4 also gives an example of the structural richness of the "second solar spectrum" (Q/I). Some of the prominent polarization features in the figure are due to various multiplets of Ti I, Cr I, C_2, and Nd II, all of which are unexpected surprises. Another strongly polarizing weak line of ionized neodynium (Nd II) has been found at 5249 Å (Stenflo & Keller 1996b).

Since each recording with the imaging CCD polarimeter (ZIMPOL) only covers about 4 Å, the more extended ranges shown in Figs. 3 and 4 have been pieced together from a series of partially overlapping recordings. In our illustrations these recordings are plotted on top of each other to allow us to judge the reproducibility of the spectral features. As can be seen, all

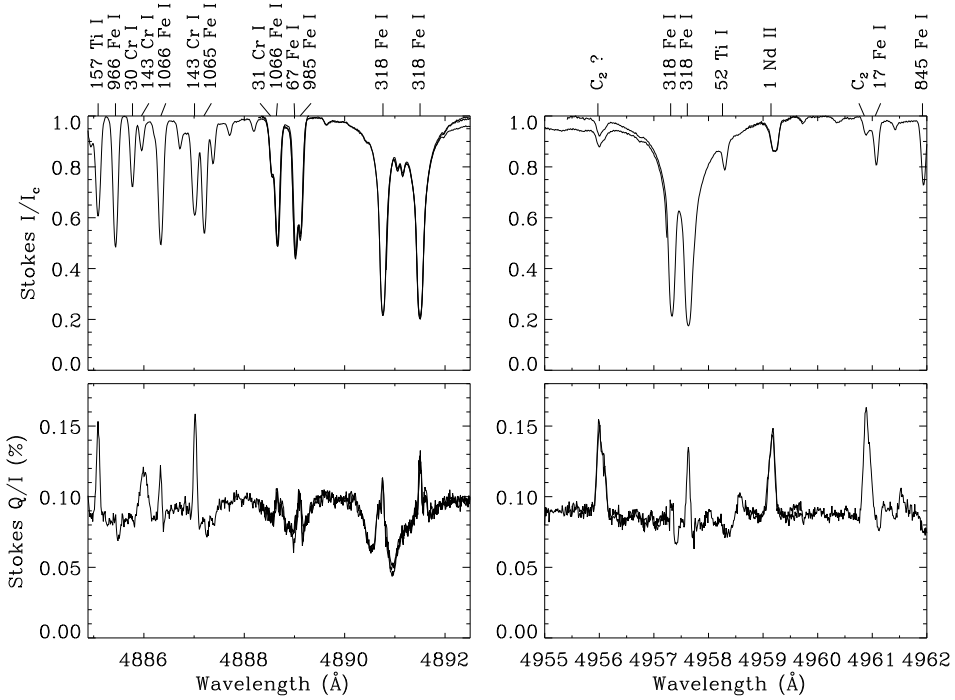

Fig. 4. Two portions of the spectrum that each contain a doublet line pair from multiplet No. 318 of Fe I. The spectra have been pieced together from separate, partially overlapping recordings (obtained in April 1995 with ZIMPOL I at NSO/Kitt Peak, 5 arcsec inside the north polar limb of the Sun), and demonstrate the high degree of reproducibility of the spectral features in the linearly polarized (Q/I) spectrum. Some of the prominent polarization features are due to Ti I, Cr I, C_2, and Nd II.

polarization features are reproduced in detail (apart from the minor high-frequency noise ripple – no Fourier filter has been applied to the data). The reproducibility is less good in the intensity spectrum (I/I_c) due to inaccurate flat-fielding of the CCD sensor (gain table effects), with efficiency gradients across the field of view. Such gain table effects divide out entirely when forming the fractional polarization (Q/I) image, which explains the better reproducibility of Q/I as compared with I alone.

The observed polarization in the 318 Fe I 4957 Å doublet has remained an enigma since it has seemed to contradict the rules of quantum mechanics. If one assumes that the two lines are formed by resonant scattering, then the 4957.302 Å line, as a $J = 4 \rightarrow 4 \rightarrow 4$ transition, should according to Eqs. (13) and (14) have a polarizability $W_2 = 0.385$, while the adjacent 4957.603 Å line, as a $J = 6 \rightarrow 5 \rightarrow 6$ transition, should have $W_2 = 0.058$. Accordingly one would expect the observed polarization amplitude of the left line of the pair to be $0.385/0.058 = 6.7$ times larger than that of the right line. The observations, both those from 1978 (Stenflo et al. 1983b) and the present ones of Fig. 4, show the entirely opposite behavior: it is the right line instead of the left one that exhibits a pronounced polarization peak, although it should have a polarizability close to zero according to its quantum numbers for resonant scattering.

The resolution of this apparent mystery comes from the fluorescent contributions, which completely change the resulting polarizabilities. Thus the emission transition $J_b = 4 \rightarrow J_f = 4$ can have three different scattering contributions: $J = 3 \rightarrow 4 \rightarrow 4$, $4 \rightarrow 4 \rightarrow 4$, and $5 \rightarrow 4 \rightarrow 4$. Similarly, the emission transition $J_b = 5 \rightarrow J_f = 6$ can have the three contributions $J = 4 \rightarrow 5 \rightarrow 6$, $5 \rightarrow 5 \rightarrow 6$, and $6 \rightarrow 5 \rightarrow 6$. These different possibilities are drawn in Fig. 1 as the dotted and dashed lines in the diagram for 318 Fe I.

With our present theory that can account for all the possible scattering contributions within a multiplet we have done some calculations to illustrate the role of fluorescence and how it can qualitatively completely change the relative distribution of polarizabilities between the various spectral lines of a multiplet. Thus the thick solid line in the upper panel of Fig. 5 has been obtained from the model of Eq. (18) when all the possible fluorescent contributions are accounted for, and we assume equal populations of all the initial states and a spectrally flat incident spectrum. The three free model parameters a, b, and the global scale factor have been adjusted to obtain a reasonable fit to the observed spectrum (represented by the thin, solid curve, taken from the lower right panel of Fig. 4).

Although the fit obtained this way is far from ideal, the model serves to illustrate what happens if we remove some of the scattering contributions. While the upper panel of Fig. 5 refers to the case when all the contributing initial states with $J_a = 3$, 4, 5, and 6 are given equal weight, the theoretical curve in the lower panel is obtained if we give zero weight to the initial states with $J_a = 3$ and 5, so that only the $J_a = 4$ and 6 states, which are the same as the final J_f states for this doublet, contribute. The relative continuum opacity and the global scaling parameter have the same values in both diagrams.

In the upper panel it is the right spectral line that dominates the polarization, in agreement with the observations, while in the lower panel it is the left line that stands out, as expected from the values of W_2 for resonant scattering. Although the lower diagram does not only have resonant contributions (the fluorescent transition $J = 4 \rightarrow 5 \rightarrow 6$ also contributes), it is dominated by the resonant contributions.

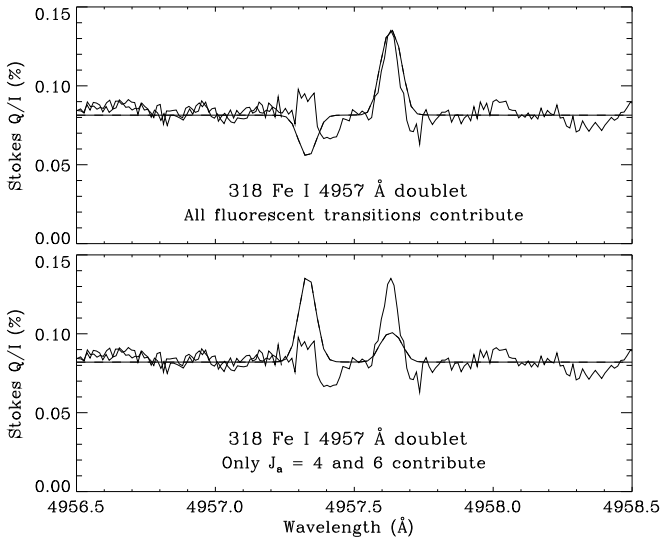

Fig. 5. Portion of the linearly polarized (Q/I) spectrum around the 318 Fe I 4957 Å doublet. The thin curves represent the observations, taken from the lower right panel of Fig. 4, while the thick curves show the results of two theoretical models. The figure serves to illustrate that the non-resonant, fluorescent contributions within a multiplet can qualitatively change the relative distribution of polarizability between the different multiplet lines.

The polarization feature of the Fe I 4957 Å doublet can thus be regarded as a signature of fluorescence effects within an atomic multiplet.

3.4. Hyperfine structure

Barium occurs in nature with a mixture of isotopes. The even isotopes, dominated by nucleon number 138, contribute 82% of the total abundance. They have zero nuclear spin and thus no hyperfine structure. The odd isotopes, dominated by isotopes 137 and 135, contribute the remaining 18% . They have nuclear spin $I = \frac{3}{2}$, like sodium nuclei. The hyperfine splitting pattern for the odd barium isotopes was shown in Fig. 1, where also the relative positions of the unsplit levels of the even isotopes were marked by the thicker, horizontal lines (neglecting the smaller isotope shifts – these shifts are however taken into account in the model calculations when weighting the contributions from the various isotopes). The atomic data used for the Ba II hyperfine structure have been taken from Rutten (1976).

Since multiplet No. 1 of Na I (with the D_1 and D_2 lines) has the same quantum numbers as multiplet No. 1 of Ba II, it also has the same hyperfine structure pattern, so the splitting diagram in Fig. 1 for the odd Ba isotopes also represents the pattern for the Na I D_2 line. The corresponding D_1 line of barium has the wavelength 4934 Å. The magnitude of the hyperfine splitting is larger in barium by about a factor of five as compared with sodium. It is the hyperfine splitting of the lower state that dominates; the splitting of the upper state is an order of magnitude smaller (cf. the different scale factors used for the lower and upper levels in the plot of Fig. 1).

For sodium the hyperfine splitting of the upper state is comparable in magnitude to the natural, radiative width (inverse life time) of the excited state. Still this minute splitting cannot be neglected since it affects the quantum interferences between the substates that determine the polarizability.

Our theory for the polarizability of multiplets can be directly applied to the case of hyperfine structure multiplets if we only substitute the quantum numbers J, L, and S with the corresponding quantum numbers F (total angular momentum), J (electronic angular momentum), and I (nuclear spin). Here we will discuss the successful application of this theory to explain the observed polarization pattern of the Ba II 4554 Å line, the "D_2 line" of multiplet No. 1 that represents a scattering transition with $J = \frac{1}{2} \rightarrow \frac{3}{2} \rightarrow \frac{1}{2}$.

Fig. 6 shows the CCD images of the observed intensity (top panel) and fractional linear polarization (bottom panel) around the Ba II 4554 Å line, recorded in April 1995 with the spectrograph slit 5 arcsec inside the Sun's north polar limb. The polarization in the Ba line exhibits a triplet structure. As will be shown below the partially resolved polarization components in the wings of the line are due to the added contributions from the hyperfine structure components of the odd isotopes, while the central component is due to the unsplit even isotopes.

Fig. 7 has been obtained from Fig. 6 by averaging along the spectrograph slit. Superposed on the Q/I diagram are two theoretical curves representing models of the polarization profile, with (thick solid curve) and without (dashed curve) quantum interferences between the split hyperfine structure levels of the excited atomic state.

The model results of Fig. 7 have been obtained, as in the Na I and 318 Fe I cases, by calculating and globally rescaling $W_{2,\,\mathrm{eff}}$ of Eq. (18) (thus for instance implicitly assuming a spectrally flat incident radiation field). When forming W_2 from Eq. (17), $C^{(2)}$ and $C^{(0)}$ have first been convolved with a Gaussian with a Doppler width of 1 km s^{-1} in velocity units, to crudely account for broadening by line of sight velocities on the Sun. For the comparison with the observations we have in addition smeared the computed W_2 profiles by convolving them with a Gaussian that has a total half width of 47 mÅ, to simulate instrumental broadening and macroturbulence. The diagram to the lower left in Fig. 2 has been obtained this way. Then a global scale factor (accounting for the geometric depolarization) has been applied to make the maxima of the observed Q/I and the scaled $W_{2,\,\mathrm{eff}}$ profiles identical.

With the so broadened and normalized $W_{2,\,\mathrm{eff}}$ function the two free parameters a and b of the model of Eq. (18) that best fit the observations have been determined. Parameter b, which represents the continuum polarization, thereby plays a subordinate role, since it mainly fixes the background polarization level that is approached at distances far from the line center. It is parameter a (the relative continuum opacity) that dominates the fitting procedure.

Our analysis shows that the partially resolved wing components of the observed polarized profiles are due to the odd barium isotopes, which appear at these wing positions due to the hyperfine structure splitting. The even isotopes, which are

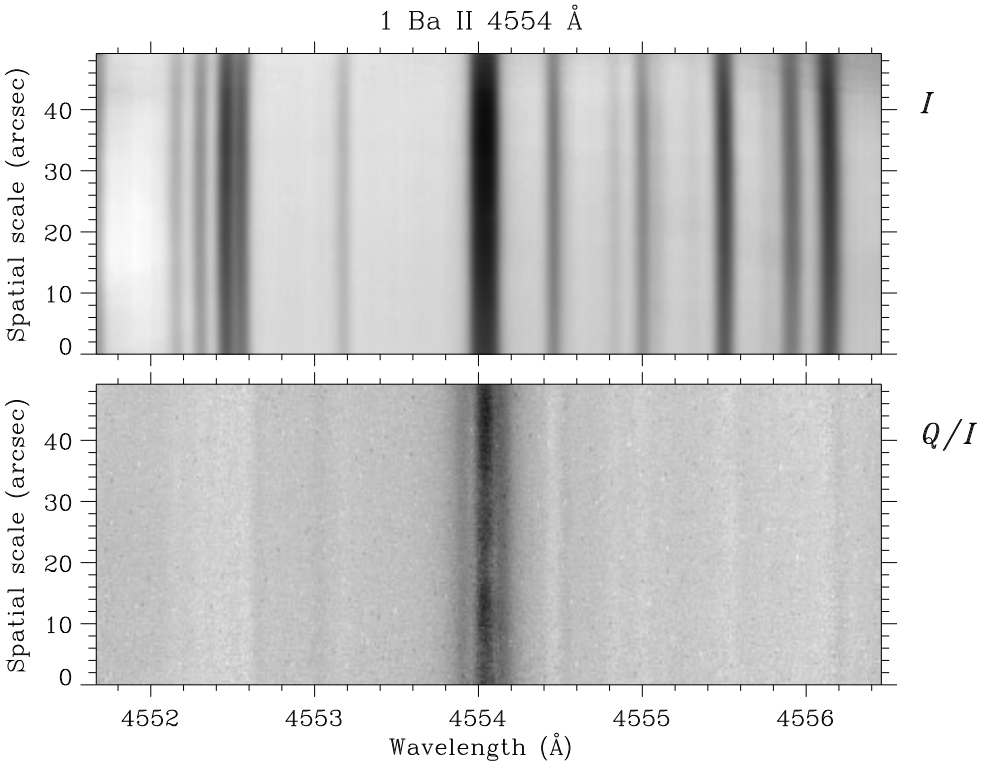

Fig. 6. Signature of hyperfine structure in barium. The images of the intensity (I) and fractional linear polarization (Q/I) were recorded in April 1995 with ZIMPOL I at NSO/Kitt Peak, with the spectrograph slit 5 arcsec inside the north polar limb of the Sun. While the central peak of the polarization triplet is due to the even isotopes, the satellite peaks in the blue and red line wings are due to the shifted hyperfine structure components of the odd isotopes.

not subject to hyperfine structure, are responsible for the central polarization peak, which is larger than the wing peaks since the relative abundance of the even isotopes is larger (82% of the total abundance). Fig. 7 also shows that quantum interferences between the split hyperfine structure components of the excited level play a significant role, although the magnitude of the splitting of the upper state is an order of magnitude smaller than that of the lower state.

Strong lines like the Ba II 4554 Å line are broadened by saturation effects when formed in an optically thick atmosphere. This broadening wipes out subtle effects in the Stokes I profiles. Such saturation does not occur for the polarization profiles. They are therefore narrower, which enhances the visibility of the hyperfine structure splitting.

4. Concluding remarks

We have seen how the physical processes that shape the second solar spectrum (Q/I) are quite different in nature from those of the ordinary intensity (Stokes I) spectrum. Examples have been given of prominent spectral signatures of quantum interference, hyperfine structure, and fluorescent scattering in the observed polarized spectrum, effects that are invisible in the normal solar intensity spectrum. The observed degree of polarization is determined by the atomic polarizability factor W_2, the ratio between the line and continuum opacities, the anisotropy of the incident radiation field, depolarizing collisions, magnetic fields (Hanle effect), etc. In general one would need to account for all these effects in a full treatment of radiative transfer with polarized scattering and partial redistribution for a numerically given model atmosphere. For initial, exploratory purposes we have introduced an idealized, parametrized model that bypasses the radiative transfer problem, ignores collisional and Hanle depolarization, and treats the effect of the anisotropy of the radiation field (geometric depolarization) as a frequency-independent scale factor.

In spite of these quite drastic idealizations it has been possible to obtain surprisingly good fits to some of the more prominent observed polarization features and to identify the underlying physics. Thus the sign reversals of the polarization curve around the Na I D_1 and D_2 lines are shown to be due to quantum interference between the $J = \frac{1}{2}$ and $\frac{3}{2}$ excited states. The apparently anomalous relative polarization amplitudes of the 318 Fe I 4957 Å doublet lines are found to be due to fluorescent contributions within the multiplet. The triplet structure of the observed polarization profile of the Ba II 4554 Å line is explained in terms of hyperfine structure splitting and relative isotope abundances.

At the same time we have identified observed polarization features that we are not yet able to explain within the framework of the present theory. While we believe that the triplet polarization peak around the core of the Na I D_2 line is primarily the result of partial redistribution effects coupled to radiative transfer, which could be modeled if a full radiative-transfer treatment with a realistic model atmosphere would be carried out, the narrow polarization peak at the center of the Na I D_1 line is an enigma. As a $J = \frac{1}{2} \rightarrow \frac{1}{2}$ transition it should be intrinsically unpolarizable at the resonant frequency (line center), and hyperfine structure in the D_1 line does not seem to help much.

The reality of the polarization peak in the Na I D_1 line is supported by observations of an even more pronounced, narrow

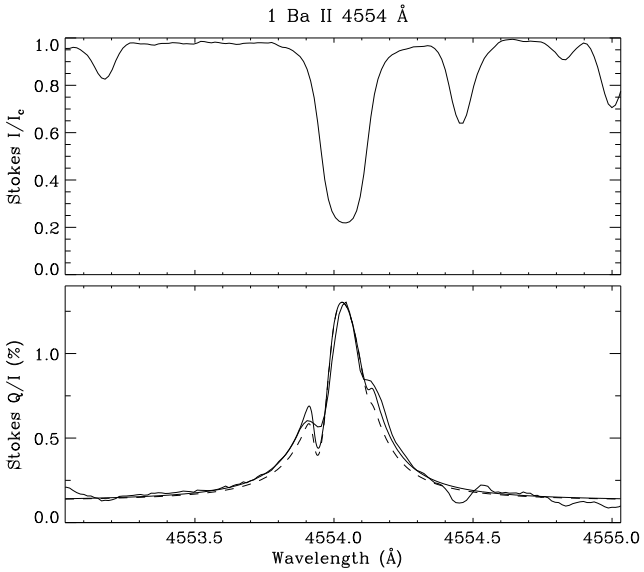

Fig. 7. 1-D version of the recording of Fig. 6, obtained by spatially averaging along the spectrograph slit. While the thin solid lines represent the observations, the thick solid and dashed curves in the Q/I diagram have been obtained with our model for the effective polarizability, $W_{2,\,\mathrm{eff}}$. The thick solid line accounts for the quantum interferences between the split hyperfine structure components of the excited state, while the dashed curve ignores the interference terms.

polarization peak in the core of the Ba II 4934 Å line (Stenflo & Keller 1996b), which is the "D_1 line" of multiplet No. 1 of Ba II, for which the 4554 Å line is the "D_2 line". Since for this multiplet the fine structure splitting is as large as 380 Å, quantum interferences between the D_2 and D_1 lines are insignificant. Furthermore, the Ba II D_1 line is less strong and deep in Stokes I as compared with the Na I D_1 line. The D_1 core polarization is thus an enigma not only for Na I, but even more so for Ba II.

One aspect that we have left out of the present treatment is the frequency redistribution problem, which needs to be dealt with before one can incorporate the present theory (which here only has been given in frequency-coherent form) in a radiative-transfer formalism with full physical realism for quantitative modelling of solar structures. Well-defined formulations of partial frequency redistribution of polarized radiation exist for single-transition Rayleigh scattering, but the generalization to multiple excited levels with quantum interferences is far from straightforward. It is for instance not clear how collisional redistribution works in the case of a mixed quantum state, like the $J = \frac{1}{2}$ and $\frac{3}{2}$ coherent superposition of the excited states of the Na I D_1 - D_2 scattering transition. Such mixed quantum states are very common.

A major simplification of the theory has been achieved by ignoring any atomic polarization of the *initial* state. This allows us to discuss the polarization properties in terms of Mueller scattering matrices or phase matrices that are decoupled from the statistical equilibrium problem. The neglect of initial-state polarization should be a very good approximation for almost all cases that will be encountered in the solar spectrum, since for spectral lines with scattering as a significant contributor to the line emission the initial state generally has such a long life that it has plenty of time to be depolarized by collisions and weak magnetic fields. The life time of the initial state with respect to radiative absorption is longer than the life time of the excited state (which is determined by the spontaneous emission rate) by approximately the Boltzmann factor $\exp(h\nu/kT)$, where T is the radiation temperature in the solar atmosphere (about 6000 K). In the visible part of the spectrum this factor is on the order of 100. Our theory could in principle readily be extended to include initial-state polarization, but the advantage that this would bring would be minor in comparison with the great technical complications it would entail. The generally far larger effects of magnetic fields, collisions, partial redistribution, and radiative transfer need to be dealt with first.

Although our theory for polarized Raman scattering with contributions from entire multiplets in principle allows for the presence of magnetic fields of arbitrary strength and direction, we have only expressed it in explicit form for the case of zero magnetic field. A major future task will be to extend the theory to provide an explicit framework that is suited for calculations that include the Hanle and Zeeman effects as well as the mixed regime of intermediately strong fields. We need to be able to handle arbitrary fields for the interpretation of the next generation of vector polarimetric observations, which will be produced by ZIMPOL II, the second generation of our imaging Stokes polarimeter. Then it will be possible to explore the local spatial fluctuations of the scattering polarization due to magnetic fields and the spectral signatures of the mixed Zeeman-Hanle regime in active regions.

The inclusion of magnetic fields in the theory leads to great technical complications because of the complex geometries (which involve the four spatial directions of the incident and scattered radiation, the magnetic field vector, and the local vertical), so certain idealized regimes will first be dealt with, like microturbulent magnetic fields (Stenflo 1982; Faurobert-Scholl 1993; Faurobert-Scholl et al. 1995). Another theoretical challenge will be to develop a sufficiently fast computer code for general multi-level polarized radiative transfer, which is flexible enough to incorporate our Raman scattering theory with magnetic fields. Since we with good reason may disregard the initial-state atomic polarization it is sufficient to treat the statistical equilibrium part of the multi-level problem with standard techniques that ignore the polarization, and then use the resulting level populations to solve the vector radiative transfer equation with the polarized scattering matrix and the absorption Mueller matrix, both of which contain the Zeeman effect. When such a tool for the solution of general polarized radiative transfer problems will become available, we will be in a position to begin to more systematically exploit the rich diagnostic potential of the second solar spectrum.

Acknowledgements. I am grateful to Christoph Keller of the National Solar Observatory, Tucson, for his support and collaboration on the observing program, and to the engineering group at ETH Zurich (Peter Povel, Peter Steiner, Urs Egger, Frieder Aebersold), who built the

ZIMPOL system and provided the technical support. It is also a pleasure to thank Veronique Bommier and Marianne Faurobert-Scholl for clarifying discussions and helpful suggestions.

Appendix A

Since the formulation and notations used in the present paper are somewhat different from those in Stenflo (1994), it may be difficult for the reader to find from that monograph the expressions for the coefficients $c(a,f)^{(K)}_{mn}$ in Eq. (9) and the exponent r in Eq. (11) for the coefficients $g(a,f)_{mn}$. As these quantities are key components of the general theory of polarized Raman scattering with quantum interferences, we give the explicit expressions here.

Let the labels m and n in $c(a,f)^{(K)}_{mn}$ be represented numerically by the differences $J_m - J_a$ and $J_n - J_a$ between the J quantum numbers of the excited and initial states, while the labels a and f are represented by the J quantum numbers of states a and f. For economy of notation we keep the name c for the function and define

$$c(J_a,J_f)^{(K)}_{J_m-J_a,\,J_n-J_a} = c(a,f)^{(K)}_{mn}\,. \tag{A1}$$

Then

$$c(J,J)^{(2)}_{-1,-1} = \frac{(J-1)(2J-3)}{30J(2J-1)(2J+1)}\,, \tag{A2}$$

$$c(J,J)^{(0)}_{-1,-1} = \frac{1}{3(2J-1)}\,, \tag{A3}$$

$$c(J,J)^{(2)}_{0,0} = \frac{(2J-1)(2J+3)}{30J(J+1)(2J+1)}\,, \tag{A4}$$

$$c(J,J)^{(0)}_{0,0} = \frac{1}{3(2J+1)}\,, \tag{A5}$$

$$c(J,J)^{(2)}_{1,1} = \frac{(J+2)(2J+5)}{30(J+1)(2J+1)(2J+3)}\,, \tag{A6}$$

$$c(J,J)^{(0)}_{1,1} = \frac{1}{3(2J+3)}\,, \tag{A7}$$

$$c(J,J)^{(2)}_{-1,0} = \frac{J-1}{10J(2J+1)}\,, \tag{A8}$$

$$c(J,J)^{(2)}_{-1,1} = \frac{2}{10(2J+1)}\,, \tag{A9}$$

$$c(J,J)^{(2)}_{0,1} = \frac{J+2}{10(J+1)(2J+1)}\,, \tag{A10}$$

$$c(J,J+1)^{(2)}_{0,0} = -\frac{2J-1}{30(J+1)(2J+1)}\,, \tag{A11}$$

$$c(J,J+1)^{(0)}_{0,0} = \frac{1}{3(2J+1)}\,, \tag{A12}$$

$$c(J,J+1)^{(2)}_{1,1} = -\frac{2J+5}{30(J+1)(2J+3)}\,, \tag{A13}$$

$$c(J,J+1)^{(0)}_{1,1} = \frac{1}{3(2J+3)}\,, \tag{A14}$$

$$c(J,J+1)^{(2)}_{0,1} = -\frac{1}{10(J+1)}\sqrt{\frac{J(J+2)}{(2J+1)(2J+3)}}\,, \tag{A15}$$

$$c(J,J+2)^{(2)}_{1,1} = \frac{1}{30(2J+3)}\,, \tag{A16}$$

$$c(J,J+2)^{(0)}_{1,1} = \frac{1}{3(2J+3)}\,. \tag{A17}$$

For symmetry reasons

$$c(a,f)^{(K)}_{mn} = c(a,f)^{(K)}_{nm}\,. \tag{A18}$$

Due to this symmetry the same off-diagonal expressions occur twice when summing over both m and n in Eq. (9). Since in the somewhat different formulation in Stenflo (1994) the double sum has been transformed to single sums, the expressions for the differently defined off-diagonal coefficients there differ by a factor of two from those here. Both definitions however lead to the identical results for $C^{(K)}_{af}$.

Another symmetry is that

$$c(f,a)^{(K)}_{mn} = c(a,f)^{(K)}_{mn} \tag{A19}$$

(symmetry with respect to reversal of the scattering direction). The symmetries (A18) and (A19) for $c(a,f)^{(K)}_{mn}$ are also valid for $g(a,f)_{mn}$ of Eq. (11).

The above algebraic expressions for $c(a,f)^{(K)}_{mn}$, together with the two symmetry relations, cover all the cases that can occur for electric dipole transitions. When a transition is not allowed, its oscillator strength is zero, which means that its $c(a,f)^{(K)}_{mn}$ factor will not contribute to the sum in Eq. (9).

The exponent r that determines the sign of the expression (11) for $g(a,f)_{mn}$ can be written as a sum of the contributions from the various transitions that are part of $g(a,f)_{mn}$. Thus

$$r = r_{am} + r_{an} + r_{fm} + r_{fn}\,. \tag{A20}$$

$r_{\ell u}$ depends exclusively on the difference $\Delta L = L_u - L_\ell$ and $\Delta J = J_u - J_\ell$ between the angular momentum quantum numbers L and J of the upper level u and lower level ℓ. We may thus write

$$r_{\ell u} = r_{\ell u}(\Delta L,\,\Delta J)\,. \tag{A21}$$

According to Stenflo (1994) the explicit expressions for all the various cases that can occur for electric dipole transitions are

$$r_{\ell u}(-1,\Delta J) = \Delta J + 1\,, \tag{A22}$$

$$r_{\ell u}(0,-1) = 0\,, \tag{A23}$$

$$r_{\ell u}(0,0) = 0 \quad \text{if} \quad J(J+1) \geq S(S+1) - L(L+1)\,, \tag{A24}$$

$$r_{\ell u}(0,0) = 1 \quad \text{if} \quad J(J+1) < S(S+1) - L(L+1)\,, \tag{A25}$$

$$r_{\ell u}(0,1) = 1\,, \tag{A26}$$

$$r_{\ell u}(1,\Delta J) = 0 \quad \text{for} \quad \Delta J = 0, \pm 1\,. \tag{A27}$$

References

Bommier, V., 1996, Solar Phys. 164, 29
Chandrasekhar, S., 1950, Radiative Transfer. Clarendon, Oxford
Condon, E.U., Shortley, G.H., 1970, The Theory of Atomic Spectra. Cambridge Univ. Press
Faurobert-Scholl, M., 1993, A&A 268, 765
Faurobert-Scholl, M., Feautrier, N., Machefert, F., Petrovay, K., Spielfiedel, A., 1995, A&A 298, 289
Frisch, H., 1996, Solar Phys. 164, 49
Keller, C.U., Aebersold, F., Egger, U., Povel, H.P., Steiner, P., Stenflo, J.O., 1992, LEST Foundation Technical Report No. 53, Univ. Oslo
Landi Degl'Innocenti, E., 1983, Solar Phys. 85, 3
Landi Degl'Innocenti, E., 1984, Solar Phys. 91, 1
Landi Degl'Innocenti, E., Bommier, V., Sahal-Bréchot, S., 1991a, A&A 244, 391
Landi Degl'Innocenti, E., Bommier, V., Sahal-Bréchot, S., 1991b, A&A 244, 401
Povel, H.P., 1995, Optical Engineering 34, 1870
Povel, H.P., Keller, C.U., Stenflo, J.O., 1991. In: November, L.J. (ed.), Solar Polarimetry. NSO/SP Summer Workshop Ser. No. 11, Sunspot, NM, p. 102
Rees, D.E., Saliba, G.J., 1982, A&A 115, 1
Rutten, R.J., 1976, Ph.D. thesis, Univ. Utrecht
Saliba, G.J., 1985, Solar Phys. 98, 1
Stenflo, J.O., 1978, A&A 66, 241
Stenflo, J.O., 1980, A&A 84, 68
Stenflo, J.O., 1982, Solar Phys. 80, 209
Stenflo, J.O., 1994, Solar Magnetic Fields – Polarized Radiation Diagnostics. Kluwer, Dordrecht
Stenflo, J.O., 1996, Solar Phys. 164, 1
Stenflo, J.O., Keller, C.U., 1996a, Nature 382, 588
Stenflo, J.O Keller, C.U., 1996b, A&A, in print
Stenflo, J.O., Baur, T.G., Elmore, D.F., 1980, A&A 84, 60
Stenflo, J.O., Twerenbold, D., Harvey, J.W., 1983a, A&AS 52, 161
Stenflo, J.O., Twerenbold, D., Harvey, J.W., J.W. Brault, 1983b, A&AS 54, 505
Stenflo, J.O., Keller, C.U., Povel, H.P., 1992, LEST Foundation Technical Report No. 54, Univ. Oslo

This article was processed by the author using Springer-Verlag LaTeX A&A style file *L-AA* version 3.